Applied Materials Today 35 (2023) 101958

Contents lists available at ScienceDirect

Applied Materials Today

journal homepage: www.elsevier.com/locate/apmt

A novel approach to the manufacture of dissolving microneedles arrays using aerosol jet printing

Hilkiah Ako [a,*], Joseph O'Mahony [a,b], Helen Hughes [a], Peter McLoughlin [a,b], Niall J. O'Reilly [a,b]

[a] Pharmaceutical and Molecular Biotechnology Research Centre (PMBRC), South East Technological University, Waterford, Ireland
[b] SSPC, the Science Foundation Ireland Centre for Pharmaceuticals, Limerick, Ireland

ARTICLE INFO

Keywords:
Additive manufacturing
3D printing
Aerosol jet printing
Dissolving microneedles
Biopharmaceuticals

ABSTRACT

Despite much research over the last few decades, microneedle arrays for the transdermal delivery of drugs have failed to live up to their initial promise. This may be changing however as companies close in on the commercial delivery of vaccines via this technology. These breakthroughs will undoubtably increase the interest in the use of microneedles arrays for the delivery of biopharmaceuticals but will also drive research into the development of scalable manufacturing processes for their fabrication. While 3D printing is an exciting development in this field, conventional Additive Manufacturing (AM) techniques are unsuitable for biopharmaceuticals due to the harsh processing conditions which can cause degradation of the active ingredient.

In this paper we report the first use of Aerosol Jet Printing (AJP) as an AM technique for the fabrication of dissolving microneedle arrays. A formulation of poly(vinyl pyrrolidone), trehalose and glycerol dissolved in water was prepared and characterised. The formulation was aerosolised using ultrasonication and deposited onto a silicon substrate. Critical process parameters such as Computer Aided Design (CAD) design, flow rate, temperature, print speed and focussing ratio were studied to determine their impact on the microneedle quality attributes. 4 × 4 microneedle arrays were printed, with needle heights > 500 μm achieved with print times of 30 mins or less. The resulting needles had sufficient strength and sharpness to penetrate porcine skin samples. Importantly, the microneedles can be fabricated under benign conditions which should be suitable for the processing and subsequent delivery of biopharmaceuticals across the skin.

1. Introduction

Biopharmaceuticals are a major driver for growth in the pharmaceutical industry, accounting for ~ 60 % of the top 50 selling drugs in 2022 [1]. Also known as biologics, these drugs include antibodies, vaccines, proteins and peptides and have proven to be very effective in the treatment of cancers, autoimmune diseases and diabetes. The vast majority of biologics are delivered parentally, which is inconvenient for the patient and often requires administration in a clinical setting. Consequently, there has been much research into alternative, less invasive delivery routes. Some progress has been made in this regard, with the pulmonary [2] and nasally [3] delivered biologics already on the market, and research ongoing into other mucosal delivery options [4]. The transdermal route is an attractive choice for drug administration, being convenient and well-accepted by patients. The large molecular size and hydrophilic nature of biologics would ordinarily rule out the transdermal delivery of macromolecules, where the outer skin layer, the stratum corneum, is a very effective barrier to drug diffusion. However numerous studies over many years have shown that proteins and peptides can be effectively delivered across the skin using microneedle array patches [5–8].

Microneedles are defined as arrays of sub-millimetre projections which are long enough to pierce the stratum corneum and embed in the lower skin layers, but too short to reach pain receptors deeper down. Therefore, they can be used for the pain-free delivery of drugs that would not normally diffuse across the skin. While many different microneedle designs and delivery mechanisms have been developed and have been comprehensively reviewed elsewhere [7–9], one of the most interesting microneedle types for the delivery of biologics is the dissolving microneedle array. Typically composed on water soluble polymers, sugars and the drug of interest, these arrays have the mechanical strength required to breach the skin but rapidly dissolve on contact with the interstitial fluid, thereby releasing the drug. On dissolution of the microneedle array, the patch can be removed from the skin, resulting in

* Corresponding author.
E-mail address: hilkiah.ako@postgrad.wit.ie (H. Ako).

https://doi.org/10.1016/j.apmt.2023.101958
Received 27 July 2023; Received in revised form 22 September 2023; Accepted 5 October 2023

minimal biohazardous waste.

Microneedle arrays have been around for almost 50 years [10], but to date there has been no medicinal microneedle array product licenced by a regulatory agency. This is in part due to challenges associated with their manufacture [6,11,12]. While some ingenious dissolving microneedle designs have been developed over the years, they invariably involve complex manufacturing techniques such as micromoulding. The advent of AM technologies or 3D printing has opened the door to another potential fabrication route for microneedle arrays. Some progress has been made in this space already. Stereolithography has been used to fabricate moulds, solid and hollow microneedles which are coated by other mechanisms such as dip coating and inkjet printing [13–15,6]. Incorporation of drug molecules during the fabrication of the needles using this method is difficult due to the limited choice of materials available and the processing conditions. Inkjet printing, another AM technique previously used to fabricate tablets [16,17], was used to coat drug molecules on to the surface of needle structures [18]. A recent study looked at fabricating silk fibroin microneedles using Digital Light Processing (DLP) [19]. DLP is an AM technique that cures materials using a UV light projector, however, the resolution obtained is based on the quality of the beam produced from the projector [20]. For all these techniques the processing conditions required are typically unsuitable for the printing of biologics which are sensitive to high temperature or photodegradation. To our knowledge no AM method has successfully produced dissolving microneedle arrays which could be used for the delivery biologics [21].

AJP is an AM technique which deposits materials in a controlled manner described by the programme file to build a 3D object. Formulations of various different materials can be prepared and deposited at viscosities between 1 and 1000 cP, which is beyond the range of other AM techniques. AJP is capable of printing features as low as 10 μm, offering freedom of design to the operator, with high precession and accuracy [22]. AJP has been used to deposit formulations on planar and non-planar surfaces due to the non-contact nature of the process [22]. For example, Gu et al. [23] demonstrated the capability of the technique in the printing of conductive silver windings over an existing conical structure. This cannot be achieved by many AM techniques currently on the market. Similarly, Goh et al. [24] deposited silver particle conductive ink using AJP to form a conformal circuit on an safety cage enclosure. An interesting study by Overmeyer et al. [25] obtained a multi-layer material sample with different hardness compositions using AJP and lasers as part of the fabrication process. Multiple atomiser chambers were used during the deposition of the materials (polymers) which again is difficult to achieve with other technologies. In the early years of its development, the technique was widely used to print electronics [26,27]. Sinha et al. [28] deposited a silver nanoparticle ink using AJP onto a polyimide substrate for electrode fabrication. Printing was achieved in 2 min and the printed part was incorporated to form a flexible multi-point fingertip sensor onto a glove. Print optimisations were carried out in a study of a metal organic silver ink to achieve homogenous lines which can be used for fabricating solar panels and light emitting electrodes [29].

3D Structures of high complexity have been fabricated using AJP. In one study, pillars were printed at different angles where the lowest angle achieved was 37° [30]. Droplet size and the rate of solvent evaporation were key factors in determining whether the structures could be assembled in such a geometry. In the same study, hollow pillars with diameters as low as 35 μm were achieved in addition to printing spiral needles of high aspect ratio forming a dome [30]. 100 hollow gold electrodes were fabricated by AJP in under 35 min, which had heights of 249 μm, a base diameter of 73 μm and top diameter of 20 μm [31]. Microelectrodes fabricated from electroless nickel immersion gold material were also fabricated using AJP to record signals [32]. Tip diameters of 20 μm were obtained and the electrodes were found to penetrate through the brains of adult C57/B6 mice. Dielectric hollow cylinders made of UV curable acrylic urethane has also been fabricated, where heights of 1.2 mm were achieved [33].

In recent times, few studies have evaluated the potential of AJP to print biological inks. DNA and proteins have been printed using AJP, where the integrity of the molecules was conserved after been atomised pneumatically [34]. Initial indications from studies suggested that ultrasonic atomisation was not a suitable method to atomise samples, as they can compromise the integrity of the molecule due to the shear forces generated in the atomisation process [34]. New research has shown that biological inks atomised by an ultrasonic atomiser does not affect the efficacy of the molecule when printed. Williams et al. [35] deposited bovine serum albumin, streptavidin, and anti-cancer embryogenic antigen antibody formulations made up in phosphate buffer solution. Findings from the study revealed that ultrasonic atomisation did not denature the proteins during printing.

In this paper we report the first use of AJP to prepare dissolving microneedle arrays using benign process conditions suitable for the deposition of biologics.

2. Materials and methods

2.1. Materials

HPLC grade water and analytical reagent grade glycerol were obtained from Fisher Scientific. Trehalose dihydrate 99 % (Acros Organics) and polyvinylpyrrolidone (PVP) with a molecular weight of 40,000 Da was purchased from Sigma Aldrich. Double sided polished silicon wafers were acquired from Entegris with a thickness of 530 ± 20 μm. Butane gas duster was purchased from RS Components. Acetone was purchased from Merck with a purity of 99.5 %.

2.2. Methods

2.2.1. Formulation preparation

An 11.11 wt% dissolving microneedle formulation for AJP deposition was prepared using a 3:1 ratio of PVP: trehalose. The components were weighed using an analytical balance (Ohaus model number PX224) and transferred into a 150 ml plastic container. 2 % of glycerol was added to the formulation based on the total weight of the polymer and sugar. 50 ml of HPLC grade water was pipetted into the container and was mixed thoroughly using a spatula. The formulation was then left to stand for 40 min to ensure all components present had dissolved.

2.3. Substrate handling

Prior to printing, silicon wafers were cut into squares, using a diamond-tipped glass cutter, which were approximately 4 cm in dimension. After the squares were obtained, the substrate was placed in acetone for 5 min. Subsequently they were sprayed with acetone and dried under nitrogen.

2.4. Viscosity

Viscometry analysis was performed using a TA AR-G2 instrument and the bob-in-cup method. The bob was a rotor-recessed concentric cylinder (27.99 mm and 42.03 mm in diameter and length, respectively). Samples were analysed at 27 °C, with a soak time of 180 s and sample analysis time of 360 s. The shear rate at which samples were analysed was varied from 0 to 1000 s^{-1}. For a guide of the dissolving microneedle formulation viscosity during aerosol deposition, the measurement was taken at 99.02 1/s. The bob gap was zeroed, the loading gap set to 9000 μm and the formulations were poured into the cup. 7.548 ml of the formulations were dispensed into the cup and the operating gap was set as 4000 μm for analysis. Viscosity measurements were carried out in triplicate.

2.5. Density

The density of the formulations was measured using an Anton Paar DMA 35 N handheld density meter using 2 ml of the formulation. The average of 6 measurements taken at ambient temperature was recorded.

2.6. Surface tension

Surface tension analysis of the dissolving microneedle formulation was carried out using the pendant drop method on a Kruss G10 contact angle measuring system at room temperature. The formulation was placed in a 3 ml syringe with a needle which had a diameter of 1.8 mm, and was dispensed until the drop was located at the tip of the needle. The drop image was captured using a focussing ratio between 5 and 10 and drop shape analysis was carried out to determine the surface tension of the formulation. The surface tension of each formulation was measured six times.

2.7. Contact angle

A Kruss G10 contact angle measuring system was used for contact angle measurements for the dissolving microneedle formulation on the substrate (silicon wafer). Measurements were carried out at room temperature using the captive bubble method. The formulation was placed into the sample compartment where the substrate was mounted onto the glass attachment. An air bubble was introduced through a needle, which had a diameter of 0.497 mm. Once the bubble was present on the substrate, the image was captured using the system. Contact angle measurements were measured by processing the image using Image J software. These were carried out 6 times and an average reading was recorded.

2.8. Computer Aided Design (CAD) drawings

All designs used in this study were drawn using AutoCAD (AutoCAD 2020, Autodesk Inc., San Rafael CA) software. Circles were used to build the microneedle structure where spacing between the needles was set to 600 μm from the centre of one circle to its neighbouring circle.

To fabricate the cylindrical type dissolving microneedles, a circle diameter of 90 μm was drawn using the software which was kept constant and repeated 60 times to build the needle structure.

To fabricate the cone like dissolving microneedles, a circle diameter of 90 μm was drawn and repeated 20 times. This was then followed by diameters of 50, 30, 20 and 10 μm with each diameter repeated 10 times resulting in a final total of 60 repetitions to build the microneedle structure.

6 dissolving lines (2 mm length each), evenly spaced at 600 μm, were printed at a single pass.

To fill the circles, the serpentine mechanism was selected using the VMTools (Virtual Machine) software. Once all designs were prepared, they were converted from "dxf" to a 'prg' to create the toolpath file which can be read by the aerosol jet printer. Microneedles were printed by depositing a layer of formulation at each of the needle positions before the next layer was deposited.

2.9. Aerosol jet printing (AJP)

Dissolving microneedle arrays were printed using an Optomec 300 Aerosol Jet Printer. Formulations were atomised via ultrasonic atomisation where 2 ml of the formulation was dispensed into a thin-walled round bottom glass vial and placed in the ultrasonic atomiser module. The temperature of the water bath in the ultrasonic atomiser module was set to 27 °C for prints used in this study. Water was added to the integrated bubbler which was approximately 1 cm above the sparger to stabilise the atomised formulation. Formulations were atomised at 0.480 A or above in this study. The aerosol mist was transported to the deposition head via a 0.385 m delivery tube using nitrogen gas. Nitrogen was also used as the sheath gas to focus the aerosol jet onto the substrate. Flow rates of the atomiser ranged from 2 to 38 ccm and the flow rate of the sheath gas ranged from 1 to 32 ccm in this study. A 300 μm nozzle was fitted to the deposition head which contained a shutter to control the deposition of the aerosolised sample onto the substrate as required. 4 mm was maintained as the working distance between the nozzle and the substrate throughout the study and print speeds varied from 0.25 to 1.25 mm/s. Substrates were cleaned prior to printing and were mounted onto the movable (X and Y direction), temperature-controlled (25–70 °C) stage. The flow sequence used during the printing process was as follows: sheath gas was powered first and after 2 min, the atomiser gas was turned on for 2 min. Finally, the atomiser power was turned on for 5 min to obtain a stable pressure prior to printing. The chamber doors of the printer were closed prior to and during each print, unless removing accumulated material collected in the shutter.

2.10. Scanning electron microscopy (SEM)

Prior to SEM analysis, samples were placed on an aluminium holder stub using double-sided carbon tape. Samples were gold coated under vacuum using a K550 Emitech sputter coater where the coating time and deposition current was set at 4 min and 50 mA, respectively. The morphology of the sample was analysed using a Hitachi S-2460 N instrument. During sample analysis, samples were analysed at an accelerating voltage of 20 kV and the emission current was set at 60 μA.

2.11. Environmental scanning electron microscopy (ESEM)

Microneedle samples were mounted on an aluminium stub using double-sided carbon tape. A Hitachi TM4000 instrument was used to analyse the morphology of the printed structures with an accelerating voltage ranging from 10 to 15 kV.

2.12. Line profilometry

A Bruker ContourX-200 was used to obtain cross sections and 3D profiles of printed lines. Prior to analysis, samples were gold coated. Cross sections of lines were approximately taken at the middle point of the line. Analysis was undertaken using a VSI (Vertical Scanning Interferometry) camera with a magnification of 1X. The back-scan and length were set at 5 and 30 μm, respectively. A threshold of 5 % was maintained where the force intensity was kept at 50 %. Data was processed using the Vision64 software.

2.13. Skin penetration studies

Pig ear samples were obtained from Dawn Pork and Bacon, Grannagh, Waterford, Ireland. The ears were placed in a beaker which contained deionised water and was left to stand for 30 min. The ears were removed from the beaker and further rinsed in deionised water to remove blood and debris on the ear. Using a scalpel, the pig skin was separated from the cartilage whilst also separating the subcutaneous layer of fat. Pig skin samples were cut into squares of approximately 4 cm in length and width and electrical trimmers were used to remove hairs in the sample.

A texture analyser (TA XT plus) was employed to test for skin penetration. Microneedle arrays fabricated by AJP were mounted on an aluminium stub using double-sided carbon tape which was then mounted to the texture analyser using a cylindrical accessory and double-sided tape. Pig skin was placed underneath the microneedle array which was lowered at a specific speed. The testing parameters were 1, 0.5 and 0.5 mm/s for pre-test, test speed and post-test speed respectively where the test mode was set as compression. The target mode of the test was set to a force of 20 N and a hold time of 30 s.

After the test was complete, methylene blue dye was applied to the

surface of the skin and allowed to stand for 10 min. Excess dye was removed from the skin using tissue paper and the skin sample was imaged using an Olympus microscope.

2.14. FTIR spectroscopy

FTIR spectroscopy was carried out using a Varaian 660 IR Spectrometer in Attenuated Total Reflectance (ATR) mode. A germanium crystal was inserted into a Varian 610 IR FTIR microscope equipped with a mercury cadmium telluride (MCT) detector. Measurements were performed in the mid-IR region (4000–600 cm^{-1}) with a spectral resolution of 4 cm^{-1}. 64 scans were taken for the background and sample. Prior to analysis, the ATR crystal was cleaned with lens tissue and the crystal was lowered until contact was made with the sample

2.15. Thermal analysis (DSC)

DSC analysis was carried out using a NETZSCH DSC 214/Polyma instrument. Approximately 2.5 mg of sample was weighed and placed into a DSC pan and sealed using a crimper. A pin hole was pierced through the lid to allow the escape of water vapour. The programme consisted of a heating and cooling cycle. The sample was heated from 20 to 250 °C at a rate of 10 °C/min. Once the temperature of 250 °C was reached, the sample was cooled down to 20 °C at the same rate. Analysis was carried out using Proteus® software.

2.16. Statistical analysis

One-way analysis of variance (ANOVA) was carried out using Minitab 20 to determine possible statistical differences in the measured heights, base diameter and tip diameter of the microneedles with respect to processing conditions used to fabricate microneedles. A P-value < 0.05 at 95 % confidence interval was considered statistically significant. Tukey analysis was carried out to determine whether the dimensions (needle height, base width diameter and tip diameter) of the microneedles obtained when fabricated under varied process conditions was statistically different.

3. Results and discussion

3.1. Formulation characteristics

A dissolving formulation developed by Dillon et al. [36] was examined in this study for its suitability to print microneedles using AJP. Their formulation consisting of 3:1 PVP: trehalose and 2 % glycerol made up in water, provides mechanical strength, rapid dissolution and offers drug stability for fabricated dissolving microneedles. Polymyxin, pentagastrin and sincalide have been incorporated in dissolving microneedles and successfully delivered using the 3:1 PVP trehalose formulation [8].

The manufacturer-recommended viscosity range for AJP using the ultrasonic atomiser is 1 −10 cP. The 11.11 wt% formulation was found to be within this range (Table 1, with flow curve data reported in Supplementary Fig. S1). Good wetting of the dissolving formulation on the acetone-cleaned silicon wafer substrate was achieved as the measured contact angles were found to be $< 90°$, which is desirable for printing (Table 1). Cader et al. [17] found that printing tablets via inkjet printing on a substrate which had a measured contact angle of 29.1 ± 2.6° resulted in the tablets adhering more to the glass substrate due to increased spreading of the deposited formulation compared to a PET substrate which had a measured contact angle of 53.4 ± 1.8° A low contact angle would be expected to be favourable in fabricating microneedles as good adhesion to the surface should make the needles more difficult to dislodge from the substrate. The surface tension of the formulation was found to be similar to a formulation used to fabricate amitriptyline hydrochloride tablets using inkjet printing where the formulation surface tension measured 62.7 mN/m [16]. Overall, the physical properties of the chosen dissolving microneedle formulation were considered to be suitable to progress to the AJP stage.

Table 1
Characteristics of prepared dissolving microneedle formulation. $N = 6$ for density, surface tension and contact angle. $N = 3$ for viscosity.

Parameter	Value
Density	1.0023 ± 0.00 g cm^{-3}
Viscosity	5.47 ± 0.02 cP
Surface tension	63.76 ± 0.25 mN m^{-1}
Contact angle	29.72 ± 0.63 °

3.2. Initial printing of dissolving microneedles

Initial scoping print runs were carried out to determine the critical process parameters and identify parameter ranges for further optimisation.

The progression of the microneedles fabricated are depicted below in Fig. 1 and the process conditions used to fabricate the needles are shown in the supplementary data Table S1. A serpentine filling pattern was used for the deposition of each layer (Fig. 1(A)) which was programmed within the CAD file. The focusing ratio, print speed and overlap in the fill influences the filling pattern. Unstable microneedles were obtained when they were fabricated at a low atomiser flow rate of 20 ccm (Fig. 1 (B)) which resulted in structures that were extremely weak and could be easily removed from the substrate using compressed gas. In addition, it was difficult to determine the interface between the microneedle base and the overspray material, which in turn made it difficult to measure the base widths of the microneedle. In Fig. 1(C) fabricated with a lower formulation concentration, the needle was broad and lacked sharpness which is problematic for skin penetration. Bulbous needle tips were obtained in Fig. 1(D) which were prepared at high print speeds. Poor reproducibility was obtained in microneedles within and between arrays when the shutter was left open during printing Fig. 1(E). Uniform needle structure was observed with no evident layers within the printed structures in Fig. 1(F) when the formulation concentration and focussing ratio were increased. Indentation can be seen at the tops of the needles and a significant amount of overspray was observed. Microneedle structures observed in Fig. 1(F) also had poor mechanical strength and were often damaged during handling for SEM analysis.

These initial runs highlighted the complexity of the deposition process and the need to carry out an in-depth study of the individual process parameters. Process optimisation was carried out where the effect of atomiser flow rate, stage temperature, printing speed and focussing ratio were analysed individually to determine conditions suitable for dissolving microneedle fabrication using AJP.

3.3. Process development for dissolving microneedle fabrication

3.3.1. Effect of atomiser flow rate on microneedle fabrication

The first stage of this work was to determine an acceptable atomiser flow rate required to deposit the dissolving formulation onto the silicon wafer substrate which would later enable the fabrication of dissolving microneedles. Atomiser flow rates direct how much material is directed to the deposition head per unit time. The quantity deposited will play a role in the drying time required for each layer. Table 2 summarises the fixed conditions used in this study when the atomiser flow was varied. The atomiser flow was increased incrementally from 2 to 36 ccm in increments of 2 ccm.

The distance between the nozzle and the substrate is known as the working distance or standoff height. Many studies have demonstrated that the optimum working distance is between 1 and 5 mm [37–39]. At distances above the recommended range, overspray present on the

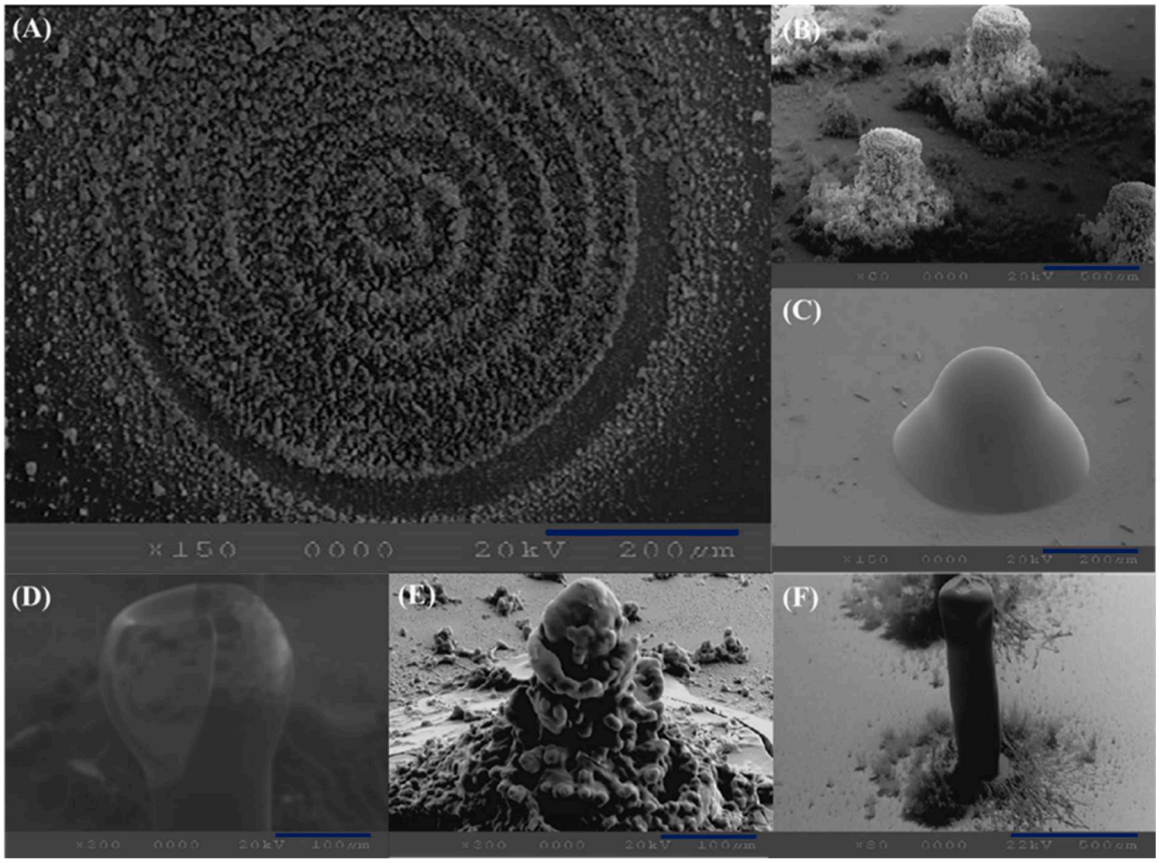

Fig. 1. Representative SEM images showing the evolution of fabricated microneedles through the means of AJP. (A) Fill pattern of layers. (D) Bulbous tip. (E) Rough needle structure (F) Needle surrounded by overspray.

Table 2
Fixed conditions for printing when varying atomiser flow.

Fixed variable	Value	Unit
Working distance	4	mm
Nozzle diameter	300	μm
Print speed	0.25	*mm*/s
Platen temperature	40	°C
Focussing ratio	1	n/a
Number of layers	1	n/a

substrate tends to greatly increase, as well as obtaining lines which are poorly defined. In this work, the working distance to the substrate base was kept constant. Given that the printed microneedles are typically 500 to 1000 μm in height, a working distance of 4 mm was used to allow a sufficient gap between the shutter and the growing microneedle. Forming of the needle tip was facilitated, as the distance is reduced each time a subsequent layer was deposited. Line widths were reduced as the working distance was decreased in a study [40]. With the distance between the nozzle and needle structure decreasing as each layer is deposited, this can aid in tip sharpness. Printing using a 300 μm nozzle was chosen to facilitate the deposition of an adequate amount of material per layer during printing. The stage temperature was maintained at 40 °C to facilitate drying of the deposited features. 37 °C was the

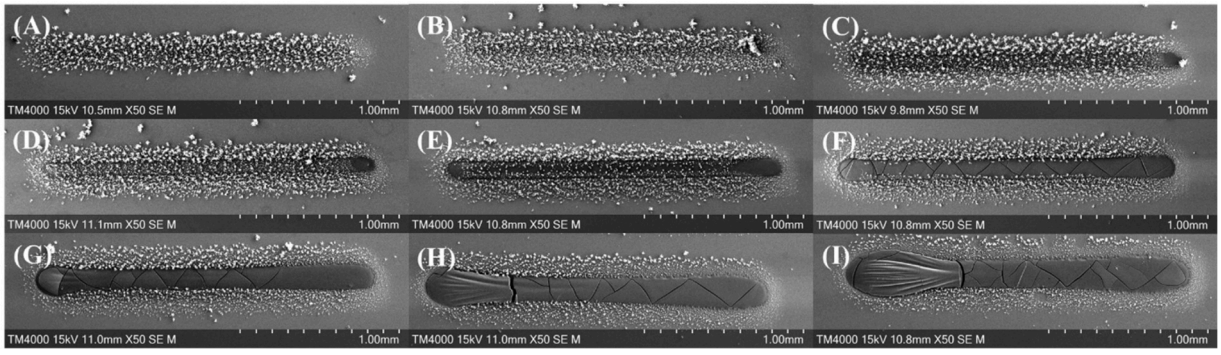

Fig. 2. SEM images of representative printed dissolving formulation lines at different flow rates with material deposition occurring from left to right in the image at a 50x magnification. (A) 20, (B) 22, (C) 24, (D) 26, (E) 28, (F) 30, (G) 32, (H) 34 and (I) 36 ccm. The fixed printing conditions were as follows; working distance 4 mm, nozzle diameter 300 μm, print speed 0.25 mm/s, platen temperature 40 °C, focussing ratio 1, number of layers 1 when printing a 11.11 wt% dissolving microneedle formulation (3:1 PVP:trehalose).

optimum stage temperature when Phuah et al. [41] deposited gelatine lines using AJP technology. Focussing ratios (i.e. the ratio of sheath gas to aerosol gas flow rate) were kept constant at 1. Lines deposited at the various atomiser flow rates are shown in Fig. 2.

Material deposition onto the substrate was not evident at flow rates below 20 ccm. Material deposition occurred on the substrate when the flow rate of the atomiser was set at 20 ccm (Fig. 2A) which resembled an aerosol mist. Difficulty in distinguishing the difference between the deposited material line and overspray was observed at flow rates between 20 and 24 ccm (Fig. 2A - C). This improved significantly as the atomiser flow rate was increased beyond 24 ccm. The line widths increased as the flow rate of the atomiser was increased. 195 ± 6 μm was the line width measured at the middle of the deposited line at the highest atomiser flow rate (36 ccm) compared to 124 ± 3 μm recorded at an atomiser flow rate of 28 ccm (Fig. 4A). Folding/ wrinkles in the deposited material was observed at the higher flow rates at above 32 ccm which progressively got worse as the flow rate was increased (Fig. 2G - I). Line widths at the beginning of the deposition were larger compared to the middle and the end of the deposition due to the initial delay when the shutter was released (Fig. 4A). For example, when the flow rate of the atomiser was set at 34 ccm, the line width at approximately 5 % of the beginning of the line was 277 ± 4 μm compared to 220 ± 11 μm at 95 % of the line.

In-plane printing was used to demonstrate the print quality after one layer of printed formulation was deposited and determine suitable flow rates for microneedle fabrication (Fig. 2). From Fig. 2A – C, very little material was deposited onto the substrate and consequently, one can rule out these flow rates which would result in weak printed structures. Similarly, in Fig. 2H – I, folding in the structure can be observed which would be expected to result in poor internal microneedle structure as insufficient drying occurs before the next layer is deposited. Following on from this in-plane study, microneedles arrays (60 layers with a CAD diameter of 90 m) were then fabricated at the same atomiser flow rates to correlate the in-plane printing results with the 3D printed structures (Fig. 3).

The fabrication of microneedles was attempted at flow rates of 20, 22 and 24 ccm. These did not have the required strength and were dislodged from the substrate base after the compressed gas post processing step and handling for SEM analysis. In-plane printing of a single circular layer showed that very little material was deposited onto the substrate and there was difficulty in distinguishing between the material deposited and overspray present on the substrate (Supplementary Data Fig. S2). The diameters of the deposited circles increased as the atomiser flow rate increased. A positive linear relationship (R^2 = 0.9906) between circle diameter and atomiser flow rate was obtained with good reproducibility (Fig. 4B).

Microneedle fabrication was facilitated at flow rates between 26 and 34 ccm. When the flow rate of the atomiser was increased there was a corresponding increase in base widths and top diameters which was statistically significant. Heights of the microneedle structures decreased as the atomiser flow rate increased. Printing of the microneedle structures at a flow rate at 36 ccm resulted in the deposition of an excess amount of material during the layering process. This led to the collapse of the needles during printing and the merging of nearby needles. The folding nature as seen in Fig. 2I was also evidenced in Fig. 3F when microneedle fabrication was attempted at the flow rate of 36 ccm. The dimensions of the fabricated microneedles at different flow rates are presented in Table 3.

Material build up in the shutter was increased at the higher atomiser flow rates which required frequent manual intervention to prevent nozzle blockage and fouling. Printing microneedle structures repeatably at flow rates of 34 ccm was not feasible as result. Flow rates of less than 28 ccm were ruled out due to their low base widths diameters. The frequency of nozzle clogging was an issue at flow rates of 26 ccm and below. Material deposition was decreased as flow rates were decreased which results in little-to-no spreading of the formulation in the shutter. Accumulation of the formulation in the shutter in an upright manner caused the build-up of the formulation to reach the nozzle tip, resulting in nozzle clogging. 32 ccm was chosen as the optimum flow rate to provide mechanical strength to fabricated microneedles and reduced clogging of the nozzle. Printing at a flow rate of 30 ccm would require the CAD diameter to be increased to match the strength of needles fabricated at 32 ccm, leading to a reduction in the resulting aspect ratio.

3.3.2. *Effect of stage temperature on microneedle fabrication*

The next stage was to determine the optimum print temperature

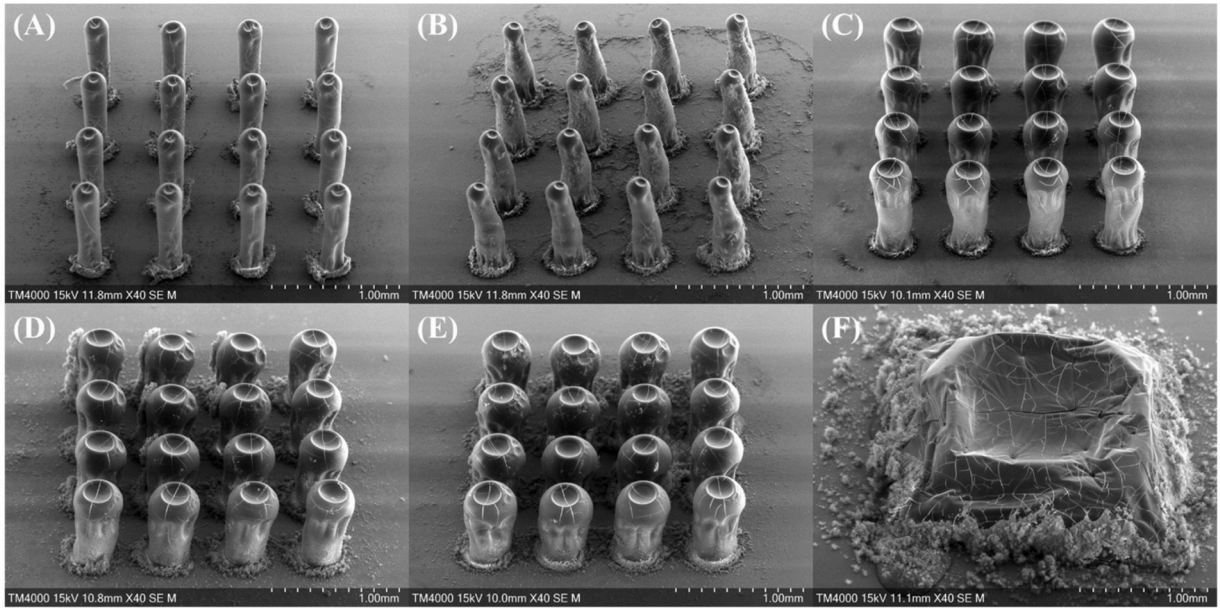

Fig. 3. SEM images of printed dissolving microneedle formulations at different atomiser flow rates. (A) 26, (B) 28, (C) 30, (D) 32, (E) 34 and (F) 36 ccm. The fixed printing conditions were as follows; working distance 4 mm, nozzle diameter 300 μm, print speed 0.25 mm/s, platen temperature 40 °C, focussing ratio 1, needle diameter as per CAD design 90 μm, number of repetitions 60 and fabrication time ~ 30 min when printing a 11.11 wt% dissolving microneedle formulation (3:1 PVP:trehalose).

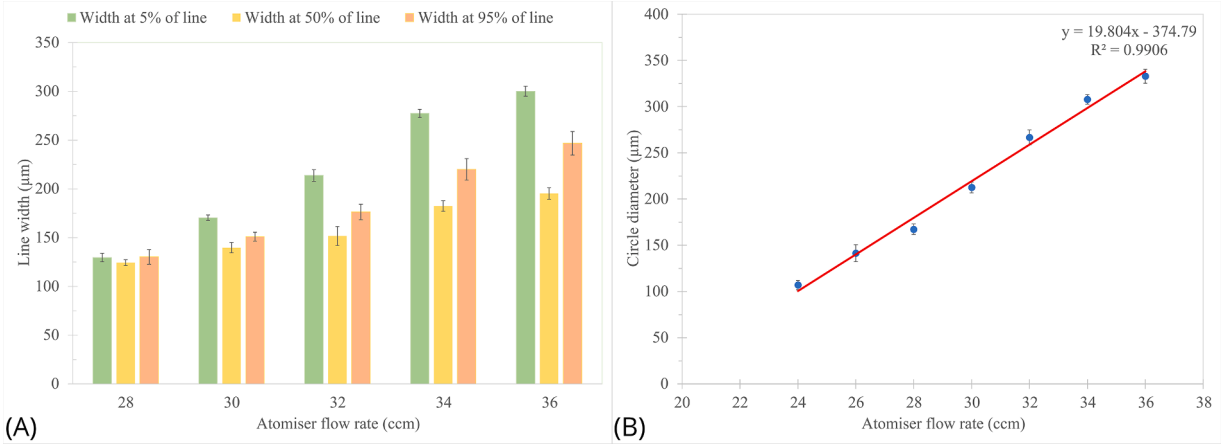

Fig. 4. (A) Effect of atomiser flow rate on line widths $n = 6$. (B) Effect of atomiser flow rate on circle diameters $n = 8$. Error bars represent +/- standard deviation.

Table 3
Effect of atomiser flow rate on printed dissolving microneedle formulation dimensions. Note: only successfully printed microneedles are reported.

Atomiser flow rate (ccm)	Column height (μm)	Base width diameter (μm)	Top diameter (μm)
26	730 ± 3^{A}	208 ± 2^{E}	202 ± 8^{D}
28	$724 \pm 6^{A,B}$	250 ± 2^{D}	185 ± 10^{E}
30	713 ± 5^{B}	289 ± 7^{C}	300 ± 8^{C}
32	699 ± 2^{C}	331 ± 5^{B}	332 ± 5^{B}
34	676 ± 7^{D}	381 ± 5^{A}	360 ± 8^{A}

Tukey analysis, where group information is displayed to show whether the dimensions of the obtained needles printed at different temperatures are statistically the same or different. Values which have been assigned the same letter in each column are considered statistically the same. $n = 4$ for height and base width diameter respectively and $n = 16$ for top diameters.

which would enable the fabrication of dissolving microneedles by depositing layers of circles to form the structure. Temperature is a parameter which can be used to control the drying rate of the deposited material. The conditions used for printing are described in Table 4 and the temperatures analysed to examine the effect on microneedle fabrication were 25, 30, 35, 40, 55 and 70 °C.

Fabrication of the dissolving microneedles at various stage temperatures is depicted in Fig. 5. The assembly of microneedles could not be facilitated at a stage temperature of 25 °C using this formulation (11.11 wt% 3:1 PVP:trehalose, Fig. 5A). Stacking of layers was achieved early on, with the structures deposited maintaining their spacing between each needle. At approx. 40 % of the total print time, the needles began to collapse and subsequently merge together as not enough heat was present to dry the early layers before the new layers cascaded and spread across the substrate. Microneedle fabrication was facilitated at a stage temperature of 30 °C (Fig. 5B). At this temperature, the lowest microneedle heights were recorded at 538 ± 2 μm. Non-uniform tips were obtained with indentation observed at the tops of the microneedles.

Table 4
Fixed conditions for printing when varying stage temperature.

Fixed variable	Value	Unit
Working distance	4	mm
Nozzle diameter	300	μm
Print speed	0.25	*mm*/s
Focussing ratio	1	n/a
Atomiser flow	32	ccm
Sheath flow	32	ccm
Needle diameter as per CAD design	90	μm
Number of layers	60	n/a
Fabrication time	~ 30	min

Uniform indentation at the tops of the microneedles were observed when the printing temperature was increased to 35 and 40 °C (Fig. 5C and B). Moreover, folding along the sides of the needle structures was observed. Heights of 589 ± 5 and 727 ± 3 μm were obtained when microneedles were printed at stage temperatures of 35 and 40 °C, respectively. Microneedle heights reached over 1000 μm when printed at stage temperatures above 40 °C. However, the incidence of nozzle clogging increased with temperatures above 40 °C. Overspray adhered more readily to the needle structures and substrate at temperatures above 40 °C (Fig. 5E and F) due to the increased drying rate. Needle heights of 1268 ± 55 μm were measured when the stage temperature was set at 70 °C, which was the tallest needles obtained in the study compared to 538 ± 2 μm when stage temperatures were set at 30 °C. Microneedle fabrication could not be completed when printing at a stage temperature of 70 °C. Due to the nature of the formulation (trehalose), increasing the stage temperature causes the formulation to stick together in the parts of the deposition head which later causes blocking. Material build up in the deposition head can be observed in Supplementary Data Fig. S3. An operating window of approximately 30 min was found when printing using conditions described in Table 4 and at a stage temperature of 70 °C which is not considered feasible for the routine printing of microneedle arrays using AJP as it would require cleaning down the heads every 30 min or so, which is time consuming.

The general trend observed was increasing the stage temperature yielded smaller base widths and smaller tip diameters. A base width of 252 ± 10 μm was measured for microneedles fabricated at a stage temperature of 70 °C compared to 335 ± 11 μm, when the temperature of the stage was 30 °C (Table 5).

Increasing the temperature of the stage resulted in less spreading of the deposited dissolving formulation on the substrate. As a result, narrower base widths were obtained which led to a corresponding increase in needle height. Temperature contributed to features obtained in dissolving microneedle fabrication using AJP. A study carried out by Herbert et al. [42] highlighted that surface roughness of deposited silver nanoparticle formulations decreased when the stage temperature was reduced.

Based on the results obtained, the stage temperature of 40 °C was considered optimal for the printing of microneedles. At this temperature, the technique is suitable for many thermolabile active ingredients which can be incorporated into the formulation to fabricate drug-loaded dissolving microneedles. The occurrence of nozzle clogging was also reduced compared to when microneedles were fabricated at 55 and 70 °C.

3.3.3. *Effect of print speeds on microneedle fabrication*

Printing speeds are another factor which can be used to influence the deposition rate of the material, with slower printing speeds increasing

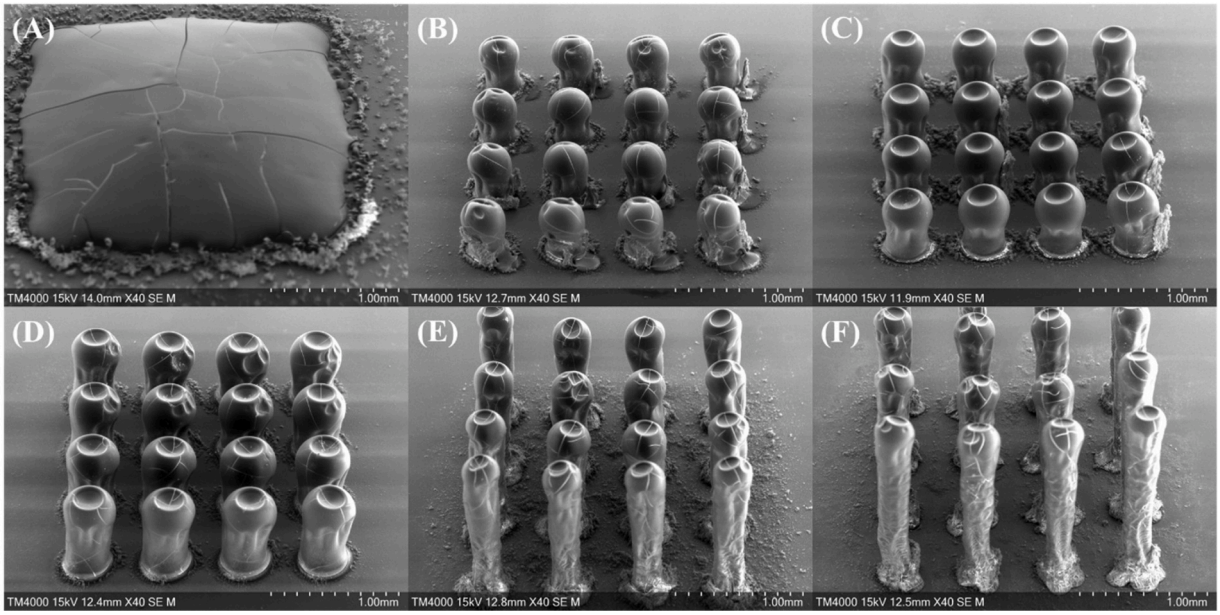

Fig. 5. SEM images of printed dissolving microneedle formulations at different stage temperatures. (A) 25, (B) 30, (C), 35 (D) 40, (E) 55 and (F) 70 °C. The fixed conditions used for printing were as follows; working distance 4 mm, nozzle diameter 300 μm, focussing ratio, 1, atomiser flow 32 ccm, sheath flow 32 ccm, needle diameter as per CAD design 90 μm, number of repetitions 60 and fabrication time ~ 30 min when printing a 11.11 wt% dissolving microneedle formulation (3:1 PVP:trehalose).

Table 5
Effect of stage temperature on printed dissolving microneedle formulation dimensions.

Temp (°C)	Column height (μm)	Base width diameter (μm)	Top diameter (μm)
25	n/a	n/a	n/a
30	538 ± 2^{D}	335 ± 11^{B}	347 ± 13^{B}
35	589 ± 5^{D}	339 ± 3^{B}	353 ± 10^{B}
40	727 ± 3^{C}	379 ± 6^{A}	393 ± 17^{A}
55	1009 ± 1^{B}	271 ± 10^{C}	317 ± 16^{C}
70*	1268 ± 55^{A}	252 ± 10^{D}	319 ± 24^{C}

* Denotes 53 layers instead of 60 layers for needle fabrication. Tukey analysis, where group information is displayed to show whether the dimensions of the obtained needles printed at different temperatures are statistically the same or different. Values which have been assigned the same letter in each column are considered statistically the same. $n = 4$ for height and base width diameter respectively and $n = 16$ for top diameters.

the deposition rate while faster print speeds would contribute to a reduction in deposited material. Previous studies have shown that the quality of printed outputs is affected when print speed was varied [29, 41]. This can possibly lead to compromises in the physical properties of the printed output. In this study, print speeds of 0.25, 0.75 and 1.25 mm/s were assessed while keeping other printing parameters constant as per Table 6.

Line profile analysis was carried out on the printed dissolving microneedle formulation (3:1 PVP: trehalose) consisting of one pass at each different print speed. In general, increasing the print speed led to a corresponding decrease in line width and line height (data not shown). Similar findings were also observed by Phuah et al. [41] when they printed lines of gelatine, although differences in line widths and heights were almost negligible when printed at higher print speeds.

The deposition rate of the formulation can be controlled by the print speeds used [43]. Faster print speeds result in a decreased deposition rate in comparison to slower print speeds. SEM images of the printed dissolving microneedle formulations at different print speeds are depicted in Fig. 6.

Fabrication times per 16-needle array decreased as printing speed was increased from 0.25 mm/s to 0.75 mm/s (30 and 23 min, respectively). There was a negligible difference in fabrication time when print speeds were increased from 0.75 to 1.25 mm/s. A statistically significant reduction in needle heights was observed with increasing print speed (Table 7). Needle heights were measured at 713 ± 6 and 809 ± 4 μm for the fastest (1.25 mm/s) and slowest (0.25 mm/s) print speeds, respectively. Needle base width diameters and top diameters showed a statistically significant decrease as print speeds were increased from 0.25 to 0.75 mm/s. Increasing the print speed further to 1.25 mm/s did not result in a change in needle dimensions. Interestingly, top diameters of the needles were larger compared to the base diameters of the needles within the array. This difference was over 100 μm at 0.25 mm/s print speed but reduced to 60 μm when the print speed was increased to 0.75 mm/s. It is possible that the moisture levels in the bottom layers were less than the levels in the top layers due to the increased contact time and closer proximity to the stage. This effect would be minimised at faster printing speeds which could account for the smaller differences in base and top diameters observed. A summary of the printed dimensions can be seen in Table 7. An increase in the amount of overspray present on the substrate and cracks within the structure of the needles were observed when printing at lower print speeds.

Needles printed at print speeds above the 0.25 mm/s analysed under the conditions used were found to be weak and could easily break during handling. For this reason, 0.25 mm/s was selected as the print speed to examine the effects of focusing ratio on the fabrication of microneedles.

Table 6
Fixed conditions for printing when varying print speeds.

Fixed variable	Value	Unit
Working distance	4	mm
Nozzle diameter	300	μm
Platen temperature	40	°C
Focussing ratio	1	n/a
Atomiser flow	32	ccm
Sheath flow	32	ccm
Needle diameter as per CAD design	90	μm
Number of layers	60	n/a

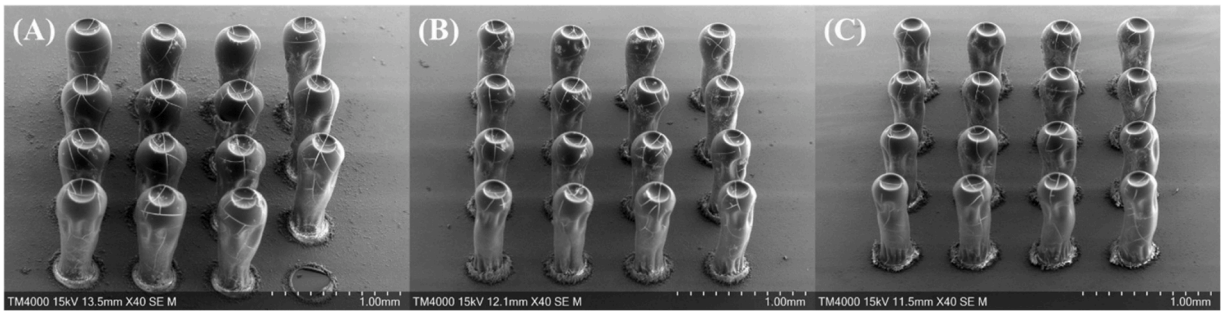

Fig. 6. SEM images of printed dissolving microneedle formulations at different print speeds. (A) 0.25, (B) 0.75 and (C) 1.25 mm/s. The fixed conditions used for printing were as follows; working distance 4 mm, nozzle diameter 300 μm, focussing ratio 1, atomiser flow 32 ccm, sheath flow 32 ccm, needle diameter as per CAD design 90 μm, number of repetitions 60 and fabrication time ≤ 30 min when printing a 11.11 wt% dissolving microneedle formulation (3:1 PVP:trehalose).

Table 7
Effect of print speeds on printed dissolving microneedle formulation dimensions.

Print speed (mm/s)	Needle height (μm)	Base width diameter (μm)	Top diameter (μm)	Print time (min)
0.25	809 ± 4^{A}	278 ± 1^{A}	391 ± 26^{A}	~ 30
0.75	767 ± 15^{B}	246 ± 6^{B}	305 ± 11^{B}	~ 23
1.25	713 ± 6^{C}	250 ± 4^{B}	302 ± 10^{B}	~ 23

Tukey analysis, where group information is displayed to show whether the dimensions of the obtained needles printed at different speeds are statistically the same or different. Values which have been assigned the same letter in each column are considered statistically the same. $n = 4$ for height and base width diameter respectively and $n = 16$ for top diameters.

3.3.4. *Effect of focusing ratio on microneedle fabrication*

Focusing ratio is the ratio of sheath gas flow rate to the atomiser flow rate. The sheath gas used is nitrogen which focuses the stream of material deposited onto the substrate. By increasing the sheath gas flow rate, higher resolution prints can be obtained. In this study, the focusing ratios analysed were 0.03, 0.5 and 1 while the other processing conditions were kept constant as reported in Table 8. For the dissolving structures to have a sharper tip to enable skin penetration, the CAD design was changed with the diameters of the circles reducing towards the latter layers (Table 8 and Fig. 8A).

Line profile analysis showed increasing the focusing ratio led to a corresponding decrease in line width but also resulted in an increase in line height, demonstrating focusing ratio plays a vital role in controlling the deposition of material in AJP (Fig. 7A and B). Moreover, flatter surfaces were obtained as the focussing ratio was increased (Fig. 7C, D and E).

Dissolving microneedles were left to stand on the stage (40 °C) for 1 h to allow the evaporation of the water present in the deposited structure. This technique is comparable to other studies which have fabricated structures using AJP process. For example, electrodes fabricated using AJP were thermally annealed for 5 h at 400 °C to remove solvent and binders in the deposited structure [31]. However, using this extreme temperature for a prolonged period of time is not suitable for the application of dissolving microneedles where drugs such as peptides and proteins will be incorporated. Microneedles fabricated at different focussing ratios are shown in Fig. 8.

Table 8
Fixed conditions for printing when varying focussing ratios.

Fixed variable	Value	Unit
Working distance	4	mm
Nozzle diameter	300	μm
Print speed	0.25	*mm/s*
Platen temperature	40	°C
Atomiser flow	32	ccm
CAD design (circle diameter)	90 μm by 20 repetitions 50 μm by 10 repetitions 30 μm by 10 repetitions 20 μm by 10 repetitions 10 μm by 10 repetitions	
Fabrication time	~ 24	min

Microneedles printed at a focusing ratio of 0.03 yielded the lowest measured needle heights and had the widest base (Fig. 8B). These needles had the least amount of overspray and it is very easy to distinguish the needle base. However, poor reproducibility was obtained in the arrays due to the lack of control when depositing the formulation. This led to needles merging together in the early deposited layers and resulted in non-uniform heights in some cases. Dents were located along the structure of the printed microneedles in addition to non-uniform indention at the tip of the needle.

Increasing the focusing ratio to 0.5 and subsequently to 1 (Fig. 8C and D, respectively), resulted in an increase in needle heights, distance from needle base to needle base and the amount of overspray present in the array. Indention at the tip of the needles is evident at these two focusing ratios with very good uniformity in needle morphology within the array. Microneedles fabricated at a focusing ratio of 1 show minor cavities/folds along the needle structure which can potentially act as an anchoring mechanism when inserted into the skin. This was more prominent compared to needles fabricated at a focusing ratio of 0.5. Tukey analysis showed that measured heights, tip diameters and base width diameters were statistically different when comparing the focusing ratios for microneedle fabrication. A summary of microneedle characteristics printed at different focussing ratios is shown below in Table 9.

3.3.5. *Functional properties of the microneedle arrays*

The dissolving characteristics of the formulations was assessed, where the fabricated AJP microneedles were observed to dissolve rapidly (< 30 s) when exposed to a droplet of water. In addition, FTIR spectra and thermal behaviour (DSC) of the printed and cast formulations highlighted no significant differences between the cast and printed formulations in both the thermograms and IR spectra. This indicates that no significant change in chemical composition occurred due to the printing process (Figs. S6 and S7, respectively).

Skin penetration studies were carried out to examine whether the fabricated microneedles at different focussing ratios could penetrate the skin. A texture analyser was used to apply the fabricated microneedles to porcine skin at a force of 20 N. Methylene blue dye was applied after the needles were pressed into the skin and used to highlight the regions of the skin penetrated by the array. This is similar to a study carried out by Park et al. [44] to demonstrate microneedle penetration. Microneedles which were fabricated at a focussing ratio of 0.03 were not attempted for the test as they lacked the sharpness and aspect ratio required (Fig. 8B). Despite smaller tip diameters obtained when a focusing ratio of 1 was used to fabricate microneedles, they failed to penetrate through the skin as the needles were dislodged from the silicon substrate during the test. Success was achieved with the needles fabricated at a 0.5 focussing ratio

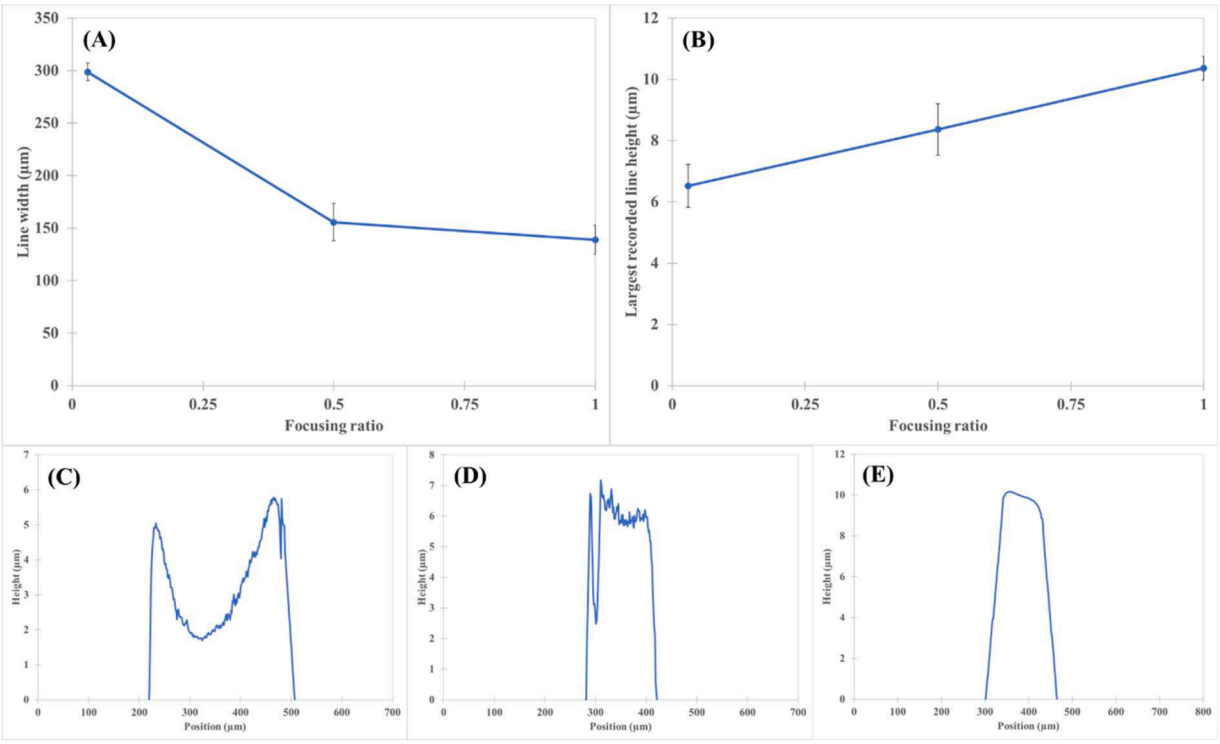

Fig. 7. (A) Effect of focusing ratio on measured line widths and (B) Effect of focusing ratio on measured line heights. Average cross sections of lines of dissolving microneedle formulation printed at different focusing ratios (C) 0.03, (D) 0.5. (E) 1. $n = 6$. Error bars represent +/- standard deviation.

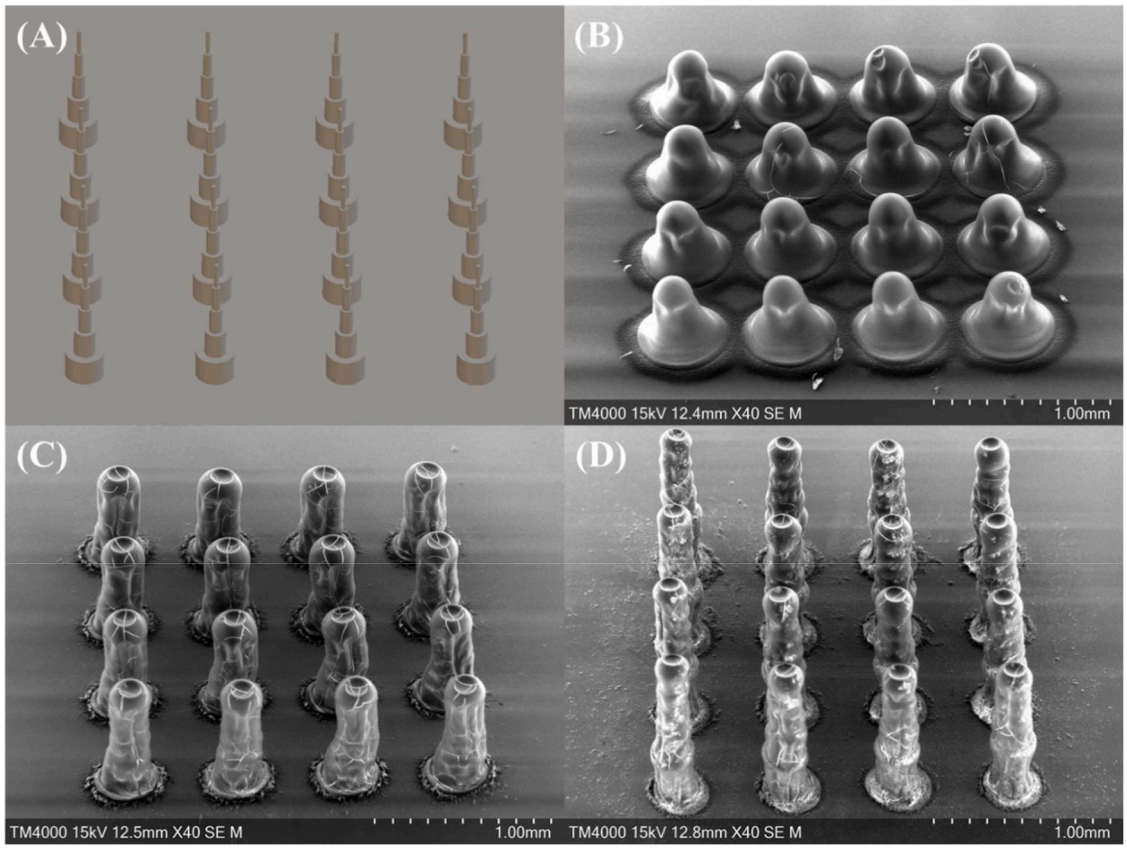

Fig. 8. SEM images of printed dissolving microneedles at different focussing ratios. (A) CAD design, (B) 0.03, (C) 0.5 and (D) 1. The fixed printing conditions are as follows; working distance 4 mm, nozzle diameter 300 µm, print speed 0.25 mm/s, platen temperature 40 °C, atomiser flow 32 ccm, 60 repetitions, fabrication time ~ 24 min when printing a 11.11 wt% dissolving microneedle formulation (3:1 PVP:trehalose).

Table 9
Effect of focussing ratios on printed dissolving microneedle formulation dimensions.

Focussing ratio	0.03	0.5	1
Needle height (μm)	514 ± 6^{A}	667 ± 4^{B}	779 ± 17^{C}
Needle width (μm)	534 ± 18^{A}	320 ± 9^{B}	253 ± 6^{C}
Tip diameter (μm)	231 ± 7^{A}	218 ± 5^{B}	171 ± 7^{C}

Tukey analysis where group information is displayed to show whether the dimensions of the obtained needles printed at different focusing ratios are statistically the same or different. Values which have been assigned the same letter in each row are considered statistically the same, values which have been assigned a different letter in each row are considered statistically different. $n = 4$ for height and base width diameter respectively and $n = 16$ for top diameters.

with 14 ± 2 ($n = 3$) of the 16 needles in the array clearly piercing the skin. This is evidenced by dye penetration test where the bright yellow spots indicate where the microneedles breached the skin and the orange colour represent regions of intact skin (Fig. 9). This, to our knowledge, is the first report of a functional dissolving microneedle array produced by AJP.

3.4. Challenges faced during microneedle fabrication and future prospects

Some of the key issues faced during the fabrication of dissolving microneedles using AJP was the formation of overspray in prints, nozzle clogging and fouling during the printing process.

Many different processing conditions were studied to obtain microneedles which could penetrate the skin. While higher focussing ratio (increasing of sheath gas flow rate) and slower print speeds yield better microneedle arrays, they were found to greatly increase the level of overspray on the substrate. Compressed gas was used as a convenient and effective post processing technique to remove overspray. Nonetheless, this can be an issue when fabricating drug-loaded microneedles as drugs present in the removed overspray will lead to the formation of biohazardous waste. Laser sintering, UV exposure and thermal annealing can be used instead of compressed gas to remove residual solvent in the deposited structure and also to improve the strength of the deposited material. Each processing technique has an effect on the characteristics of the printed structure. Laser sintering and UV exposure are not ideal methods to fabricate dissolving microneedles. UV exposure can cause the formation of free radicals which may degrade the drug while for laser sintering, the solvent and or components must absorb in the IR region. Thermal annealing was used in one study to reduce the presence of overspray on printed nickel nanoparticle film lines [38]. If thermal annealing is to be used as part of the dissolving microneedle fabrication, temperatures used must not cause degradation of the drug and materials present in the formulation.

Considerable challenges were associated with printing structures when the flow rate of the atomiser was 30 ccm and above for the dissolving microneedle formulation. Nozzle fouling was the biggest issue when printing the structures over a prolonged period of time. Fouling can be defined as unwanted material being deposited onto the substrate. Occasionally an uncontrolled amount of the formulation was deposited onto the substrate which ruins the print. This could be due to a number of issues such as nozzle clogging and or a build-up of the formulation around the nozzle (Fig. 10). Due to the sugar (trehalose) present in the mixture, it can sometimes lead to "spin sugar" being formed starting at the tip of the nozzle or shutter and cause contamination of the print. This is the main reason why the working distance was set to 4 mm to reduce the occurrence of this happening, a larger distance from shutter to nozzle would prevent the nozzle being in contact with the formulation collected in the shutter. Reitberger et al. [45] identified the maximum flow rate of the atomiser to be 1200 sccm when depositing clear varnish through a 300 μm diameter when the stage temperature was 45 °C. At atomiser flow rates above 1200 sccm, droplets began to form on the tip of the nozzle which later caused nozzle fouling. Manual intervention was employed after fabricating each array to remove formulation build up in the shutter using a micro pipette to reduce the likelihood of the nozzle clogging and fouling occurring. It was found during print trials that successful printing occurred during an operating window between 3 and 4 h before fouling occurs when printing under the conditions described in Section 3.3.4 and manually removing build up in the nozzle. A build-up of aerosol droplets in the delivery tube contributed to this fouling. It is also worth noting that the success rate of microneedle fabrication using the technique was also affected by the cleanliness of the substrate. Poor cleanliness resulted in the deposited material spreading from the position set in the programme file. This leads to different height measurements and base dimensions of the resulting needles.

Although out of the scope of the current paper, limited work has been published in the area of printed biological inks using the technique. As

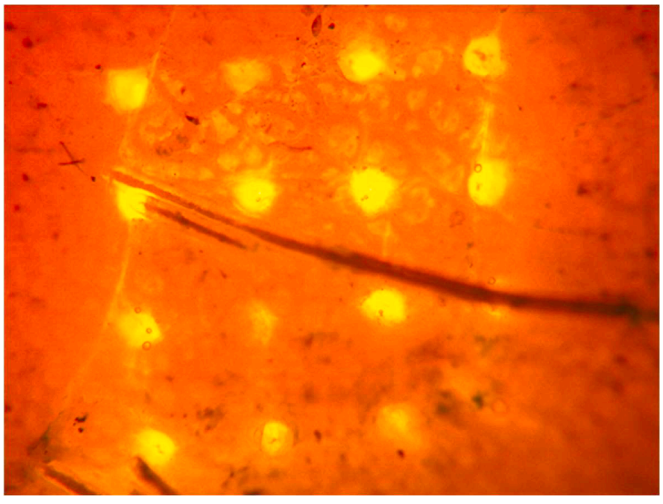

Fig. 9. Representative image of porcine skin after microneedle insertion fabricated at a focusing ratio of 0.5.

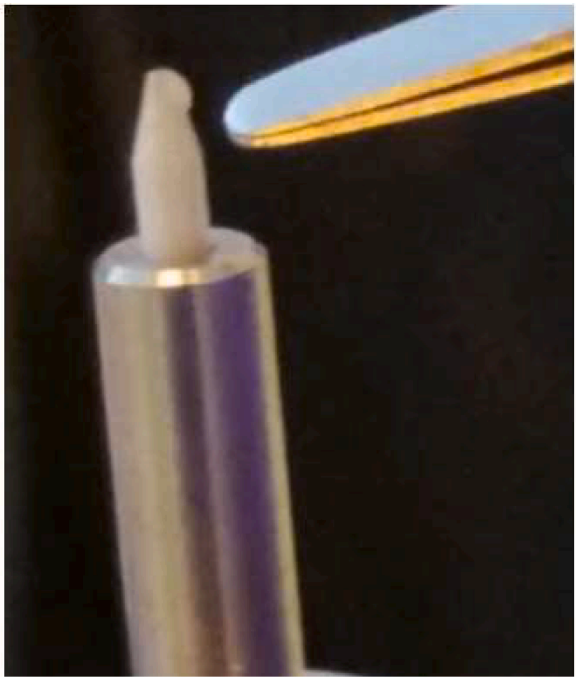

Fig. 10. Build-up of dried dissolving microneedle formulation at the tip of the nozzle.

mentioned previously, promising results from Williams et al. [35] have shown that denaturation of proteins (bovine serum albumin, streptavidin, and anti-cancer embryogenic antigen antibody formulations) did not occur when deposited by ultrasonic atomisation using the AJP process.

The use of this technology for bioprinting is in its infancy. The work presented here highlights a novel method for fabricating dissolving microneedles which has been difficult to achieve using standard 3D printing techniques such as SLA due to limited choice of materials available. AJP offer greater flexibility in terms of atomisation options, formulation components, resolution and the ability to process a wide range of formulation viscosities. While microneedle fabrication using AJP has been demonstrated, scale up of the current process is out of scope of this paper. Multiple print heads can be attached to the instrument to increase the fabrication output. Ali et al. [31] printed a 100-electrode array with heights of 200 μm within 35 min. Simultaneous printing using four printheads was found to decrease this time by 7 – 8 min per array.

Additionally, materials being printed are cheap relative to other 3D printing techniques and allows customisation depending on the release profiles required. Ultimately, the AJP of dissolving microneedles may be beneficial in niche applications, for drug products required by small patient populations or where its flexibility and programmable nature would be advantageous, such as in the production of personalised medicines.

4. Conclusions

To the best of our knowledge, we report for the first time the fabrication of dissolving microneedle arrays using AJP with ultrasonic atomisation. A 3:1 PVP: trehalose mixture containing 2 % glycerol and HPLC grade water as the solvent was deposited using AJP on a silicon wafer to fabricate microneedles. The physical properties of the formulation such as viscosity, density, surface tension and substrate contact angle were characterised prior to printing. A systematic approach was carried out to examine the effects of each process condition individually to determine their impact on print quality. The atomiser flow rate, print speed, focussing ratio and stage temperature were evaluated to generate 4×4 microneedle array with adequate mechanical properties. Microneedles dimensions were 667 ± 4 μm for height, base diameter of 320 ± 9 μm and 218 ± 5 μm for the tip diameter when a focusing ratio of 0.5 was used for fabrication. These biocompatible sugar polymer microneedles were found to penetrate the skin.

While much optimisation is required for realising commercial microneedle fabrication, the work here clearly demonstrates that AJP can be used to produce dissolving microneedle arrays with the requisite properties to penetrate the skin using relatively benign processing conditions. This opens up the possibility of incorporating biomolecules into the formulation and printing dissolving arrays suitable for the delivery of peptides, proteins, antibodies and vaccines.

CRediT authorship contribution statement

Hilkiah Ako: Conceptualization, Data curation, Methodology, Investigation, Formal analysis, Writing – original draft. **Joseph O'Mahony:** Conceptualization, Methodology, Supervision, Validation, Writing – review & editing. **Helen Hughes:** Conceptualization, Supervision, Validation, Writing – review & editing. **Peter McLoughlin:** Conceptualization, Supervision, Validation, Writing – review & editing. **Niall J. O'Reilly:** Conceptualization, Funding acquisition, Project administration, Supervision, Validation, Writing – original draft, Writing – review & editing.

Declaration of Competing Interest

The authors declare that they have no known competing financial interests or personal relationships that could have appeared to influence the work reported in this paper.

Data availability

Data will be made available on request.

Acknowledgments

The authors would like to thank Dr. Vasil Stoichkov for the initial training of the printer. The authors would like to thank Dr. Colin Reidy, Mr. Bruno Zluhan and Mr. Arun Antony, SETU, for their help with the line profilometry work. The work conducted in this research article was funded by the Irish Research Council (GOIPG/2022/1682) and South East Technological University (grant WIT/PhD/2019/002).

Supplementary materials

Supplementary material associated with this article can be found, in the online version, at doi:10.1016/j.apmt.2023.101958.

References

[1] B. Buntz, The 50 best-selling pharmaceuticals of 2022: COVID-19 vaccines poised to take a step back, Drug Discov. Dev. (2023). Apr. 18, https://www.drugdiscoverytrends.com/50-of-2022s-best-selling-pharmaceuticals/ (accessed Jul. 14, 2023).
[2] W. Liang, H.W. Pan, D. Vllasaliu, J.K.W. Lam, Pulmonary delivery of biological drugs, Pharmaceutics 12 (11) (2020) 1–28, https://doi.org/10.3390/pharmaceutics12111025.
[3] J. Rohrer, N. Lupo, A. Bernkop-Schnürch, Advanced formulations for intranasal delivery of biologics, Int. J. Pharm. 553 (1–2) (2018) 8–20, https://doi.org/10.1016/j.ijpharm.2018.10.029.
[4] J. Das Neves and B. Sarmento, Mucosal delivery of biopharmaceuticals: biology, challenges and strategies, vol. 9781461495246. Springer US, 2014. doi:10.1007/978-1-4614-9524-6.
[5] G. Du, et al., Intradermal vaccination with hollow microneedles: a comparative study of various protein antigen and adjuvant encapsulated nanoparticles, J. Control. Release 266 (2017) 109–118, https://doi.org/10.1016/j.jconrel.2017.09.021.
[6] C.P.P. Pere, et al., 3D printed microneedles for insulin skin delivery, Int. J. Pharm. 544 (2) (2018) 425–432, https://doi.org/10.1016/j.ijpharm.2018.03.031.
[7] H.S. Gill, M.R. Prausnitz, Coated microneedles for transdermal delivery, J. Control. Release 117 (2007) 227–237, https://doi.org/10.1016/j.jconrel.2006.10.017.
[8] C. Dillon, H. Hughes, N.J. O'Reilly, C.J. Allender, D.A. Barrow, P. McLoughlin, Dissolving microneedle based transdermal delivery of therapeutic peptide analogues, Int. J. Pharm. 565 (2019) 9–19, https://doi.org/10.1016/j.ijpharm.2019.04.075.
[9] D. Nicholas, et al., Rapid paper based colorimetric detection of glucose using a hollow microneedle device, Int. J. Pharm. 547 (2018) 244–249, https://doi.org/10.1016/j.ijpharm.2018.06.002.
[10] M.S. Gerstel and V.A. Place, "Drug delivery device," 3, 964, 482, 1976.
[11] J.W. Lee, M.R. Prausnitz, Drug delivery using microneedle patches: not just for skin, Expert Opin. Drug Deliv. 15 (6) (2018) 541–543, https://doi.org/10.1080/17425247.2018.1471059.
[12] A.M. Rodgers, A.J. Courtenay, R.F. Donnelly, Dissolving microneedles for intradermal vaccination: manufacture, formulation, and stakeholder considerations, Expert Opin. Drug Deliv. 15 (11) (2018) 1039–1043, https://doi.org/10.1080/17425247.2018.1522301.
[13] R.D. Boehm, P.R. Miller, S.L. Hayes, N.A. Monteiro-Riviere, R.J. Narayan, Modification of microneedles using inkjet printing, AIP Adv. 1 (2) (2011) 1–13, https://doi.org/10.1063/1.3602461.
[14] I. Xenikakis, et al., Fabrication and finite element analysis of stereolithographic 3D printed microneedles for transdermal delivery of model dyes across human skin in vitro, Eur. J. Pharm. Sci. 137 (2019), https://doi.org/10.1016/j.ejps.2019.104976.
[15] V. Yadav, et al., 3D printed hollow microneedles array using stereolithography for efficient transdermal delivery of rifampicin, Int. J. Pharm. 605 (2021), https://doi.org/10.1016/j.ijpharm.2021.120815.
[16] K. Sen, A. Manchanda, T. Mehta, A.W.K. Ma, B. Chaudhuri, Formulation design for inkjet-based 3D printed tablets, Int. J. Pharm. 584 (2020), https://doi.org/10.1016/j.ijpharm.2020.119430.
[17] H.K. Cader, et al., Water-based 3D inkjet printing of an oral pharmaceutical dosage form, Int. J. Pharm. 564 (2019) 359–368, https://doi.org/10.1016/j.ijpharm.2019.04.026.
[18] S. Ross, N. Scoutaris, D. Lamprou, D. Mallinson, D. Douroumis, Inkjet printing of insulin microneedles for transdermal delivery, Drug Deliv. Transl. Res. 5 (4) (2015) 451–461, https://doi.org/10.1007/s13346-015-0251-1.

[19] D. Shin, J. Hyun, Silk fibroin microneedles fabricated by digital light processing 3D printing, J. Ind. Eng. Chem. 95 (2021) 126–133, https://doi.org/10.1016/j.jiec.2020.12.011.
[20] I. Gibson, D.W. Rosen, and B. Stucker, Additive manufacturing technologies: 3D printing, rapid prototyping, and direct digital manufacturing. 2010. doi:10.1007/978-1-4419-1120-9.
[21] U. Detamornrat, E. McAlister, A.R.J. Hutton, E. Larrañeta, R.F. Donnelly, The role of 3D printing technology in microengineering of microneedles, Small 18 (2022), https://doi.org/10.1002/smll.202106392.
[22] J. Hamre and K. D'Arezzo, "Aerosol Jet ® UA max ultrasonic atomizer user manual," 2013.
[23] Y. Gu, D. Park, D. Bowen, S. Das, D.R. Hines, Direct-write printed, solid-core solenoid inductors with commercially relevant inductances, Adv. Mater. Technol. 4 (2019), https://doi.org/10.1002/admt.201800312.
[24] G.L. Goh, et al., Fabrication of designoptimized multifunctional safety cage with conformal circuits for drone using hybrid 3D printing technology, Int. J. Adv. Manuf. Technol. 120 (2022) 2573–2586.
[25] L. Overmeyer, A. Hohnholz, O. Suttmann, S. Kaierle, Multi-material laser direct writing of aerosol jet layered polymers, CIRP Ann. Manuf. Technol. 68 (1) (2019) 217–220, https://doi.org/10.1016/j.cirp.2019.04.115.
[26] T. Seifert, M. Baum, F. Roscher, M. Wiemer, T. Gessner, Aerosol jet printing of nano particle based electrical chip interconnects, Mater. Today Proc 2 (8) (2015) 4262–4271, https://doi.org/10.1016/j.matpr.2015.09.012.
[27] C. He, N. Jin, H. Yu, J. Lin, C.Q. Ma, The electrical sintering and fusing effects of aerosol-jet printed silver conductive line, Mater. Lett. 246 (2019) 5–8, https://doi.org/10.1016/j.matlet.2019.03.016.
[28] A.K. Sinha, G.L. Goh, W.Y. Yeong, Y. Cai, Ultra-low-cost, crosstalk-free, fast-responding, wide-sensing-range tactile fingertip sensor for smart gloves, Adv. Mater. Interfaces 9 (21) (2022), https://doi.org/10.1002/admi.202200621.
[29] R. Eckstein, G. Hernandez-Sosa, U. Lemmer, N. Mechau, Aerosol jet printed top grids for organic optoelectronic devices, Org. Electron. 15 (9) (2014) 2135–2140, https://doi.org/10.1016/j.orgel.2014.05.031.
[30] M.S. Saleh, C. Hu, R. Panat, Three-dimensional microarchitected materials and devices using nanoparticle assembly by pointwise spatial printing, Sci. Adv. 3 (3) (2017) 1–8, https://doi.org/10.1126/sciadv.1601986.
[31] M.A. Ali, et al., Sensing of COVID-19 antibodies in seconds via aerosol jet nanoprinted reduced-graphene-oxide-coated 3D electrodes, Adv. Mater. 33 (2021), https://doi.org/10.1002/adma.202006647.
[32] M.S. Saleh, et al., CMU array: a 3D nano-printed, customizable ultra-high-density microelectrode array platform, Sci. Adv. 8 (40) (2019), https://doi.org/10.1101/742346.
[33] T. Rahman, R. Panat, D. Heo, 3-d antenna structures using novel direct-write additive manufacturing method, in: Proceedings of the International Technical Conference and Exhibition on Packaging and Integration of Electronic and Photonic Microsystems, 2015, pp. 1–5.
[34] I. Grunwald, et al., Surface biofunctionalization and production of miniaturized sensor structures using aerosol printing technologies, Biofabrication 2 (1) (2010), https://doi.org/10.1088/1758-5082/2/1/014106.
[35] N.X. Williams, N. Watson, D.Y. Joh, A. Chilkoti, A.D. Franklin, Aerosol jet printing of biological inks by ultrasonic delivery, Biofabrication 12 (2) (2020), https://doi.org/10.1088/1758-5090/ab5cf5.
[36] C. Dillon, H. Hughes, N.J. O'Reilly, P. McLoughlin, Formulation and characterisation of dissolving microneedles for the transdermal delivery of therapeutic peptides, Int. J. Pharm. 526 (2017) 125–136, https://doi.org/10.1016/j.ijpharm.2017.04.066.
[37] B. Clifford, D. Beynon, C. Phillips, D. Deganello, Printed-sensor-on-chip devices – aerosol jet deposition of thin film relative humidity sensors onto packaged integrated circuits, Sens. Actuators B Chem. 255 (2018) 1031–1038, https://doi.org/10.1016/j.snb.2017.08.086.
[38] H. Zhang, J.P. Choi, S.K. Moon, T.H. Ngo, A hybrid multi-objective optimization of aerosol jet printing process via response surface methodology, Addit. Manuf. 33 (2020), https://doi.org/10.1016/j.addma.2020.101096.
[39] Y.D. Chen, V. Nagarajan, D.W. Rosen, W. Yu, S.Y. Huang, Aerosol jet printing on paper substrate with conductive silver nano material, J. Manuf. Process 58 (2020) 55–66, https://doi.org/10.1016/j.jmapro.2020.07.064.
[40] A. Mahajan, C.D. Frisbie, L.F. Francis, Optimization of aerosol jet printing for high-resolution, high-aspect ratio silver lines, ACS Appl. Mater. Interfaces 5 (11) (2013) 4856–4864, https://doi.org/10.1021/am400606y.
[41] E.W.C. Phuah, W.L. Hart, H. Sumer, P.R. Stoddart, Patterning of biomaterials by aerosol jet printing: a parametric study, Bioprinting 18 (2020), https://doi.org/10.1016/j.bprint.2020.e00081.
[42] R. Herbert, S. Mishra, H.R. Lim, H. Yoo, W.H. Yeo, Fully printed, wireless, stretchable implantable biosystem toward batteryless, real-time monitoring of cerebral aneurysm hemodynamics, Adv. Sci. 6 (18) (2019), https://doi.org/10.1002/advs.201901034.
[43] P. Kopola, et al., Aerosol jet printed grid for ITO-free inverted organic solar cells, Sol. Energy Mater Sol. Cells 107 (2012) 252–258, https://doi.org/10.1016/j.solmat.2012.06.042.
[44] S.C. Park, M.J. Kim, S.K. Baek, J.H. Park, S.O. Choi, Spray-formed layered polymer microneedles for controlled biphasic drug delivery, Polymers 11 (2) (2019), https://doi.org/10.3390/POLYM11020369 (Basel).
[45] T. Reitberger, G.A. Hoffmann, T. Wolfer, L. Overmeyer, J. Franke, Printing polymer optical waveguides on conditioned transparent flexible foils by using the aerosol jet technology, in: Proceedings of the Printed Memory and Circuits II, SPIE, 2016, https://doi.org/10.1117/12.2236220.